Chapter 2
Catalysis

Hervé Jobic

Abstract Catalysis helps to save energy and to produce less waste. Hydrogen will possibly be the energy carrier for the future, but it will not replace oil before several decades so the efficiency of the catalytic processes in petroleum refinery and petrochemistry still has to be improved. Numerous physical techniques are being used to follow catalytic processes. The samples can be subjected to several probes: electrons, photons, ions, neutrons; and various fields can be applied: magnetic, electric, acoustic, etc. Apart from the basic catalyst characterization, the various methods aim to observe surface species (intermediate species are much more tricky), the reaction products, and the influence of diffusion. Coupling of two, three, or more techniques is now common and very powerful. The biggest challenge has always been to perform measurements during the reaction, the term in situ being sometimes replaced by the more recent one operando, when the catalyst is under working conditions of pressure, temperature, flow, and avoiding diffusion limitations.

2.1 Catalysis and Neutron Scattering

The main classes of heterogeneous catalysts are: (i) metals and alloys (supported or not), (ii) metallic oxides (including mixed oxides, heteropolyacids, superacids), (iii) zeolites and molecular sieves in general, and (iv) sulfides. It will take some more years before deciding if metal-organic frameworks (MOFs) become a new member of the catalysts family.

Several neutron techniques are used to study catalytic systems: neutron diffraction (ND), small-angle neutron scattering (SANS), inelastic neutron scattering (INS), and quasi-elastic neutron scattering (QENS). We will limit ourselves here to INS and QENS of hydrogen species and dihydrogen molecules adsorbed on the surface of catalyst particles or inside porous materials.

H. Jobic (✉)
Centre National de la Recherche Scientifique, Institut de Recherches sur la Catalyse et l'Environnement de Lyon, Lyon, France
e-mail: herve.jobic@ircelyon.univ-lyon1.fr

G.J. Kearley and V.K. Peterson (eds.), *Neutron Applications in Materials for Energy*, Neutron Scattering Applications and Techniques,
DOI 10.1007/978-3-319-06656-1_2

Hydrogen has recently been associated with the words fuel cells and energy storage, but it is also an essential component in catalytic reactions and the hydrogen produced is mainly used in petroleum refining and ammonia production for fertilizer. Nowadays, about 90 % of the H_2 production comes from catalytic steam reforming of natural gas at high temperatures (subsequent reactions of water–gas shift and preferential oxidation are required to decrease the CO level of the gas mixture to a few ppm before it can be used in a fuel cell). At the time being, one is facing a huge increase of H_2 needs (with related CO_2 emissions), so that until Jules Verne's predictions are realized (water: the coal of the future), we may reach an H_2 deficit, as predicted by some experts.

The applications of INS to catalysis have been mainly focused to systems which are either difficult or impossible to study by other spectroscopies such as transmission or reflection–absorption infrared, and Raman. The kind of catalyst which is studied in INS has generally an inhomogeneous surface, e.g. oxides, sulfides, and metals, although zeolites, which are well-crystallized materials, are well suited. These substrates can be almost transparent to neutrons if they contain a small quantity of hydrogen, in which case the neutron spectrum will be fairly flat and it will be possible to observe all the vibrational modes of the adsorbate.

QENS has been mainly used to measure the diffusion of H or hydrogenated molecules, although the transport of deuterated molecules and of molecules which do not contain hydrogen atoms can now be followed. The dimensionality of diffusion has been studied, even if the samples are in powder form. On zeolites [1], MOFs [2], or clays [3], anisotropic diffusion (one or two dimensional) has been evidenced. The technique allows us to probe diffusion over length scales ranging from an Å to hundreds of Å. The mechanism of diffusion can thus be followed from the elementary jumps between adsorption sites to Fickian diffusion.

2.2 Neutron Spectroscopy of Hydrogen-Containing Materials

There are very few works on atomic-hydrogen diffusion on catalysts by QENS, the H species resulting from H_2 dissociation have been predominantly studied by INS. When hydrogen is bonded to metal atoms, the heavy atoms can be considered as fixed during the local modes of hydrogen. A consequence is that the mean-square amplitudes for the hydrogen atoms will be generally small so that the sample temperature will be of small influence on the INS intensities. Another consequence is that the nondegenerate modes of hydrogen will have nearly the same intensity and an E mode will be twice as intense as an A mode. The INS spectra can thus be fitted and the relative intensities of the bands yield the populations of the various sites.

INS studies of the adsorption of H_2 on various materials, to observe rotational transitions, and of various hydrogen species present on metal and sulfide catalysts were previously reviewed [4, 5]. Only recent work will be considered here.

2.2.1 Sorption of H_2 During the Reduction of Copper Chromite

The activation of a copper–chromium system in H_2 is accompanied by an accumulation of H_2, which can become active for hydrogenation reactions, in the absence of H_2 in the gas phase. This sorption of H_2 is due to a specific mechanism of Cu^{2+} reduction from the $CuCr_2O_4$ structure, a reaction which does not release water. The reduction leads to the formation of metallic copper and to protons substituting for copper cations in the vicinity of O^{2-} anions. INS spectra of copper chromite as prepared and reduced at various temperatures are shown in Fig. 2.1. The initial catalyst shows bands at low frequencies, due to the mass of the atoms, these bands having a low intensity because no proton motion is involved. Upon reduction, a large intensity

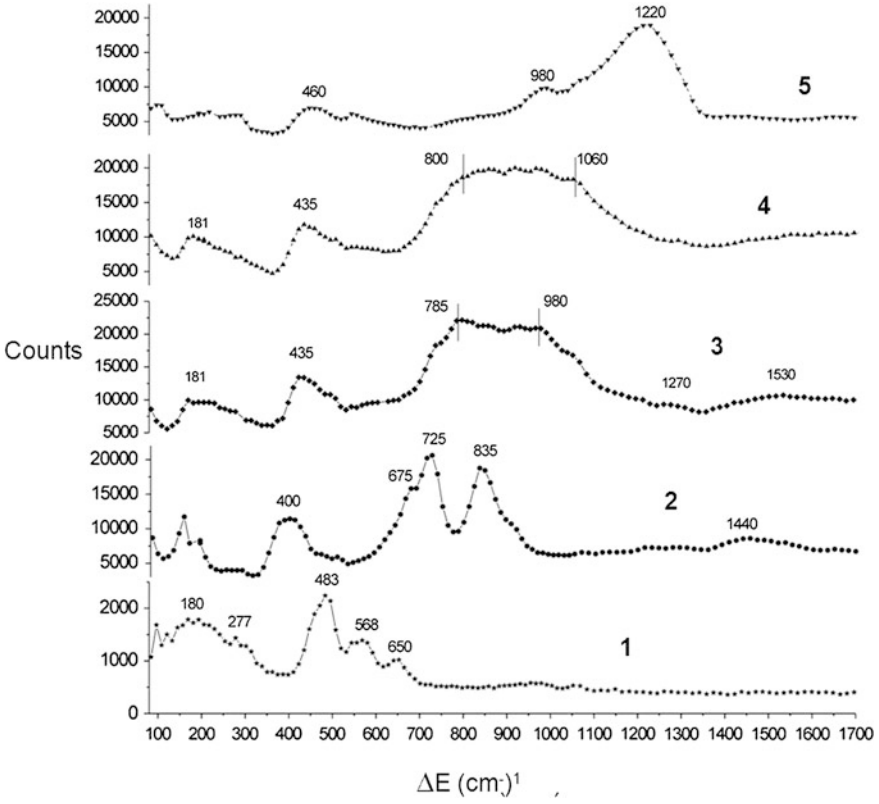

Fig. 2.1 INS spectra of as prepared and reduced samples of copper chromite. *1* Initial spectrum, *2* reduced with hydrogen at 250 °C, *3* at 290 °C, *4* at 320 °C, *5* at 450 °C. The data were obtained on the instrument IN1BeF at the Institut Laue–Langevin (ILL). Adapted with permission from (A.A. Khassin, G.N. Kustova, H. Jobic, T.M. Yurieva, Y.A. Chesalov, G.A. Filonenko, L.M. Plyasova, V.N. Parmon, Phys. Chem. Chem. Phys. **11**, 6090 (2009)) [6]

increase can be measured and OH-groups bending modes are observed in the energy range displayed in Fig. 2.1. Increasing the reduction temperature yields a shift of these bending modes to higher frequencies (from 700–800 to 1,220 cm^{-1}), while the stretching modes shift to lower energy. This indicates that hydrogen bonding strength with neighbouring anions increases with the rise in temperature. The band around 400 cm^{-1} was assigned to librations of two geminal protons (i.e. HOH-groups) [6].

2.2.2 *Dissociation of H_2 on Ceria-Supported Gold Nanoparticles*

Catalysis by Au nanoparticles has attracted considerable attention since it was discovered that Au particles, with a size less than a few nm, are active. Au nanoparticles deposited on oxides can dissociate H_2 heterolytically on sites involving one Au atom and a nearby surface oxygen atom. This is in contrast with other metals such as M = Ni, Pd, Pt, etc., where H_2 is dissociated homolytically (in a symmetric fashion). The relatively poor activity of Au for hydrogenation reactions was attributed partly to the inability of Au to break the H–H bond and to the instability of Au hydrides (Au–H species), while various M–H species have been clearly evidenced by INS.

The INS spectra obtained after chemisorption of H_2 on 3–4 nm Au particles supported on nanoparticulate ceria (5 nm) show a peak at 400–600 cm^{-1} accompanied by a broad band from 750 to 1,200 cm^{-1}. The first peak was assigned to bridging hydroxyl groups, and the second band to librational modes of water present on the catalyst surface and resulting from the reaction of hydrogen with oxygens of ceria [7]. The lack of observation of Au–H species by INS can be explained by the low percentage of Au on the sample (Au loading: 0.48 wt%). On the other hand, the formation of Au–H could be observed by Fourier-transform infrared (FT-IR) spectroscopy, which seems to indicate a greater sensitivity of IR spectroscopy for this sample.

2.2.3 *Hydride Species in Cerium Nickel Mixed Oxides*

Bio-ethanol obtained from biomass has been suggested as a promising renewable source of H_2. It is a challenge to find low-cost catalysts (without noble metals) able to break the C–C bond of ethanol at low temperature. A $CeNiH_ZO_Y$ catalyst was recently found to convert ethanol at 60 °C only, by steam reforming coupled with partial oxidation [8]. The distribution of products is similar to what is obtained by steam reforming at high temperatures: H_2 (about 45 %) and mainly CO_2 and CO. The reaction is initiated at 230 °C, but the temperature increases after a short induction period so that a temperature of 60 °C is sufficient to maintain the reaction. This is explained by the occurrence of two exothermic reactions: (i) between hydride species

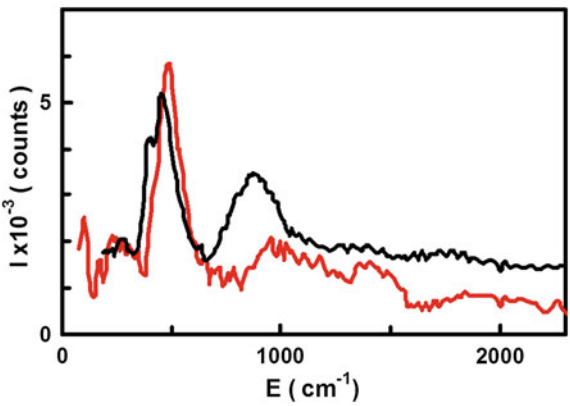

Fig. 2.2 INS spectra of $CeNi_1O_Y$ (*black*) and $CeNi_{0.5}O_Y$ (*red*/*grey*) after a treatment at 250 °C under H_2 (the INS spectrum of the solid treated in vacuum at 200 °C was subtracted). The data were obtained on the instrument IN1BeF at the ILL

of the catalyst and O_2, and (ii) between ethanol and O_2 (partial oxidation). The reaction is sustainable because hydride species are replaced and provided by ethanol.

A pre-treatment at 250 °C under H_2 is necessary to obtain the active catalyst, which is an oxyhydride. As in the case of copper chromite, large quantities of hydrogen can be stored in $CeNi_XO_Y$ mixed oxides. H_2 is heterolytically dissociated at an anionic vacancy and an O^{2-} species of the catalyst. The insertion of hydride species in the solid was evidenced by INS. The spectra of $CeNi_1O_Y$ and $CeNi_{0.5}O_Y$ are shown in Fig. 2.2. The INS spectrum of the solid treated in vacuum at 200 °C, which contains OH groups, has been subtracted. The peak at about 460 cm^{-1} was assigned to hydrides and the band around 870 cm^{-1} to H adsorbed on metallic Ni particles, because the band intensity decreases when the Ni loading is decreased. While the assignment of the first peak appears to be reliable (after re-oxidation, this peak disappears whereas a band corresponding to OH groups emerges around 630 cm^{-1}), the assignment of the higher frequency band to μ_3-H species on Ni^0 particles is less certain, and the contribution from OH groups cannot be excluded.

2.3 Dihydrogen

In the long term, H_2 is envisaged as a potential energy carrier. However, one of the issues for portable applications of this energy vector relies on its economic and safe pressure storage under the conditions of transport. Although the targets set for 2015 by the U.S. department of energy (DOE) are difficult to reach, several options are extensively investigated. Compressed or liquefied H_2 is not suitable for mobile applications, because of low volumetric energy density and safety problems. A promising way for mobile applications is solid state storage. One can differentiate physisorption in porous materials, including zeolites, MOFs and different types of carbons, and chemisorption resulting in the formation of hydrides. INS has been used to characterize various hydrides, starting from transition-metal hydrides, up to complex hydrides composed with light elements (lithium, boron, sodium or aluminium),

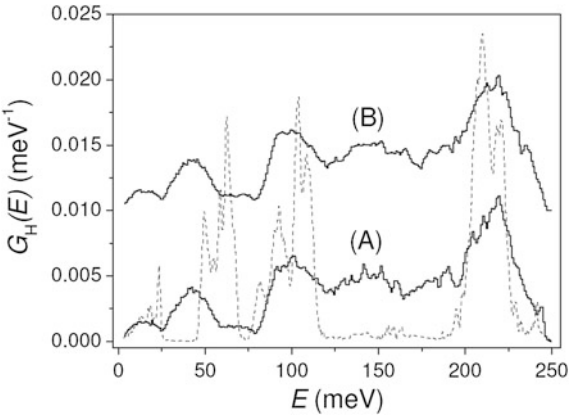

Fig. 2.3 INS spectra from $NaAlH_4$/ACF-25: **A** as prepared, **B** after hydrogen desorption–absorption cycling (*full lines*); the *dashed line* corresponds to bulk $NaAlH_4$. The data were recorded on the instrument TOSCA, at the pulsed neutron and muon source at the Rutherford Appleton Laboratory (ISIS). Reprinted with permission from (D. Colognesi, A. Giannasi, L. Ulivi, M. Zoppi, A.J. Ramirez-Cuesta, A. Roth, M. Fichtner, J. Phys. Chem. A **115**, 7503 (2011)) [11]

which provide high gravimetric H_2 density. Catalysts play a role in some cases: for alanates, doping with a titanium catalyst increases the rates of adsorption and desorption of H_2 [9], for borohydrides, hydrogen release through a hydrolysis reaction can be controlled catalytically [10].

Since transport can be a limiting step, the use of nanoparticles is an option to improve the kinetics. Raman scattering and INS techniques have been used to find out if the infiltration process of a carbon matrix with $NaAlH_4$ creates new chemical species (e.g., Na_3AlH_6) and if the nanoparticles of $NaAlH_4$ have a physical state different from the bulk or not [11]. The influence of hydrogen desorption–absorption cycling was also tested. The INS spectra of the melt-infiltrated composite of $NaAlH_4$ and active carbon fibers (ACF-25) are compared to the corresponding spectroscopic data taken from bulk $NaAlH_4$ in Fig. 2.3.

The comparison between spectra (a) and (b) in Fig. 2.3 indicates that INS is not sensitive to the desorption–absorption cycle. On the other hand, the comparison with bulk $NaAlH_4$ shows a broadening of the peaks with some energy shifts, typical of crystal-size effects. The extra intensity observed between 130 and 200 meV was attributed to the presence of a small amount of Na_3AlH_6, also observed in the Raman spectrum [11].

2.3.1 Hydrogen Diffusion in Nanoporous Materials

Atomic hydrogen diffusion in metal lattices has been studied for a long time by QENS, e.g. [12]. The diffusion of atomic hydrogen on the surface of catalysts has

been studied scarcely [13, 14], this could be revisited since the neutron flux and the instrumentation has been tremendously improved since. Dihydrogen diffusion in porous media is a more recent topic. H_2 diffusion is of interest for a number of industrial processes, including membranes for fuel cells or reactions with membrane reactors, where the zeolite acts as a porous membrane. Over the last years, a large number of studies have been conducted on MOFs, to explore the performance of these solids as energy carrier for H_2. In general, for applications involving gas separation, a fast diffusion rate of the gas molecules into the porous system is as important as the adsorption uptake, the selectivity, or the regenerability.

There are few measurements on the diffusion of H_2 in zeolites and MOFs, this is due to the difficulty in measuring fast sorption rates by macroscopic methods. There are also few theoretical studies, a classical approach being not sufficient at low temperatures since the de Broglie thermal wavelength is comparable to the diameter of the confining pores, requiring in this case a quantum mechanical treatment.

The self-diffusivity, D_s, of H_2 in several zeolites was studied by pulsed-field gradient nuclear magnetic resonance (PFG-NMR) and QENS [15]. The self-diffusion coefficients were found to decrease with decreasing pore sizes of the zeolite structures, with one notable exception in silicalite. In this case, the diffusivities were found to be exceptionally small, the explanation being that H_2 molecules are trapped within the pentasil chains forming the structure.

While the self-diffusivity can be determined from incoherent neutron-scattering, the transport diffusivity, D_t, can be derived from coherent neutron-scattering [16]. Normally, D_t is measured under the influence of concentration gradients, i.e. under non-equilibrium conditions. It may seem strange to derive a non-equilibrium quantity from experiments performed at equilibrium. This is because the scattering function corresponding to coherent scattering is related to the full correlation function, $G(\mathbf{r}, t)$, which is itself connected with the evolution of the particle density around equilibrium. This approach was already formulated by Onsager [17] in his regression hypothesis. It was later proven that the response of a system to an external perturbation can be evaluated from correlation functions of the sample at equilibrium.

For a comparison of the different results, the transport diffusivity is often represented in terms of the so-called corrected diffusivity, D_0, which is defined by the relation

$$D_t(c) = D_0(c)\left(\frac{d\ \ln p}{d\ \ln c}\right) \tag{2.1}$$

where c denotes the adsorbate concentration in equilibrium with the pressure p. The term $d\ln p/d\ln c$ is the thermodynamic factor. When the adsorption isotherms can be fitted with the Langmuir model, the thermodynamic factor is equal to or larger than 1 [18].

2.3.1.1 Simultaneous Measurement of Self- and Transport Diffusivities

Deuterium is a special case for neutrons since it has comparable coherent and incoherent cross-sections. With D_2 molecules, it is then possible to measure simultaneously D_s and D_t. Such an experiment was performed for different concentrations of D_2 adsorbed at 100 K in the NaX zeolite [19]. The self-diffusivities were checked from the broadenings measured at the same loadings for H_2, after correcting from the mass difference between the two isotopes.

The values of D_s are plotted in Fig. 2.4. The slight increase of the self-diffusivity which is observed when the concentration increases was initially attributed to an interaction with the sodium cations [19]. This was later confirmed by atomistic computer simulations on the basis of the loading dependence of the partial molar configurational internal energy of the sorbate molecules, which indicated the existence of low-energy sites which are preferentially filled at low occupancy [20]. Molecules residing in these sites tend to exhibit lower translational mobility than molecules sorbed elsewhere in the intracrystalline space at higher occupancy.

The values of D_t, obtained at the same loadings, are also reported in Fig. 2.4. The width of the coherent scattering was found to show a minimum corresponding to the maximum of the structure factor. This line narrowing is characteristic of quasi-elastic coherent scattering and was first predicted by de Gennes [21].

It appears that at low D_2 concentration, the self- and transport diffusivities are similar, but for higher loadings the transport diffusivity increases rapidly and exceeds the self-diffusivity, as expected from the contribution of the thermodynamic factor, Eq. (2.1). This means that the lattice gas model, which predicts that the transport diffusivity does not depend on the concentration, does not apply for this system. Only close to the saturation of the zeolite does the transport diffusivity

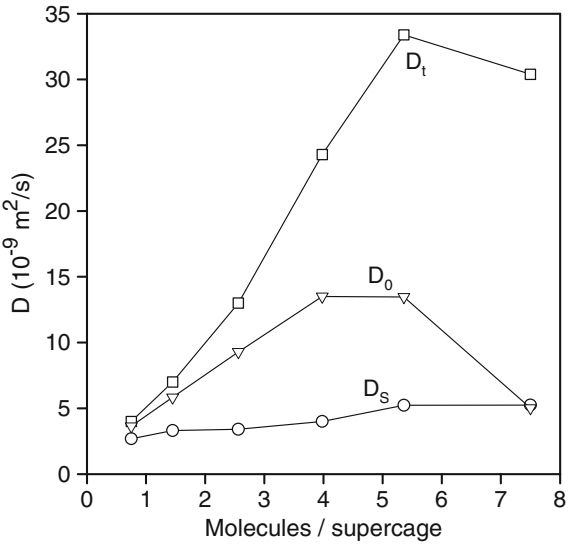

Fig. 2.4 Different diffusion coefficients obtained for D_2 in NaX zeolite at 100 K, as a function of loading: (*squares*) transport diffusivity, (*triangles*) corrected diffusivity, and (*rounds*) self-diffusivity

start to decrease, indicating that collective motions become affected by the packing density. The corrected diffusivity, D_0, was obtained from D_t and from the thermodynamic factor calculated by fitting a Langmuir isotherm to the adsorbed quantities. It is clear from Fig. 2.4 that for D_2 in NaX the corrected diffusivity is not constant, this assumption being often made in the interpretation of macroscopic measurements.

2.3.1.2 Diffusion of Hydrogen in One-Dimensional Metal-Organic Frameworks

MIL-53(Cr), and its isostructural form MIL-47(V), are built up from infinite chains of corner-sharing $Cr^{3+}O_4(OH)_2$ or $V^{4+}O_6$ octahedra interconnected by 1,4-benzenedicarboxylate groups (Fig. 2.5). These three dimensional MOFs contain one-dimensional diamond-shaped channels with pores of nm dimensions. One may note that MIL-53(Cr) exhibits hydroxyl groups located at the metal–oxygen–metal links (μ_2-OH groups) which open up the possibility of additional preferential adsorption sites and thus different adsorption or diffusion mechanisms to that of MIL-47(V) where these specific groups are absent.

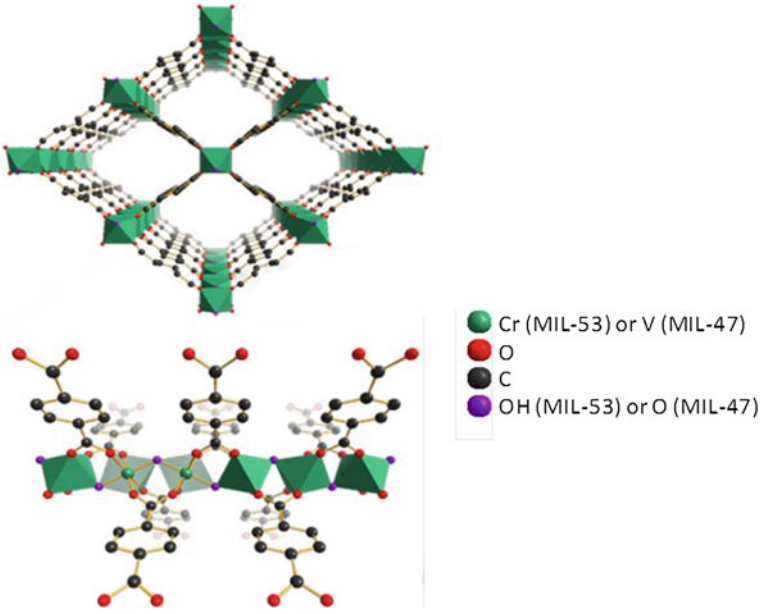

Fig. 2.5 View of the MIL-47(V) and MIL-53(Cr) structures. *Top* view along the chain axis, highlighting the one-dimensional pores system; *bottom* chain of corner sharing $Cr^{3+}O_4(OH)_2$ or $V^{4+}O_6$ octahedra

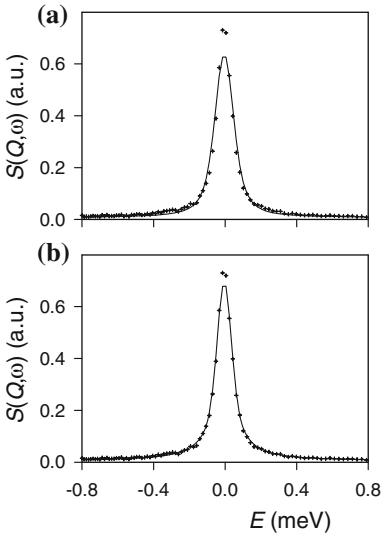

Fig. 2.6 Comparison between experimental (*crosses*) and fitted QENS spectra obtained for H_2 in MIL-53(Cr) at 77 K; the *solid lines* are computed for **a** three-dimensional diffusion, and **b** one-dimensional diffusion (Q = 0.27 Å^{-1}, 3.5 molecules per unit cell on average). The spectra were measured on the IN6 instrument at the ILL. Adapted with permission from (F. Salles, D.I. Kolokolov, H. Jobic, G. Maurin, P.L. Llewellyn, T. Devic, C. Serre, G. Férey, J. Phys. Chem. C **113**, 7802 (2009)) [22]

The self-diffusion of H_2 in these two structures was studied by QENS combined with molecular dynamics (MD) simulations [2, 22]. For the QENS measurements, the frameworks and the μ_2-OH groups in MIL-53(Cr) were deuterated to reduce the signal from the MOF. To illustrate the possibility to obtain information on diffusion anisotropy, one and three dimensional diffusion models are compared with experimental spectra in Figs. 2.6 and 2.7. When the diffusion is isotropic (three-dimensional), the theoretical dynamic structure-factor, $S(Q, \omega)$, corresponding to a translational motion has a Lorentzian profile in energy, but the line shape is more elongated in the case of diffusion in one-dimensional channels, because a powder average has to be made [22].

In MIL-53(Cr), profiles corresponding to three-dimensional diffusion and convoluted with the instrumental resolution do not fit perfectly through the experimental points (Fig. 2.6a and Ref. [22] for spectra obtained at other Q values). A normal one-dimensional diffusion model, with a more waisted shape, fits better the experimental data (Fig. 2.6b and Ref. [22]). This is due to the interaction between H_2 and the μ_2-OD groups, leading to a one-dimensional diffusion along the tunnels via a jump sequence involving these hydroxyl groups. Normal one-dimensional diffusion means that the molecules can cross each other in the tunnels of MIL-53. When the molecules cannot pass each other, the diffusion is called single file [23].

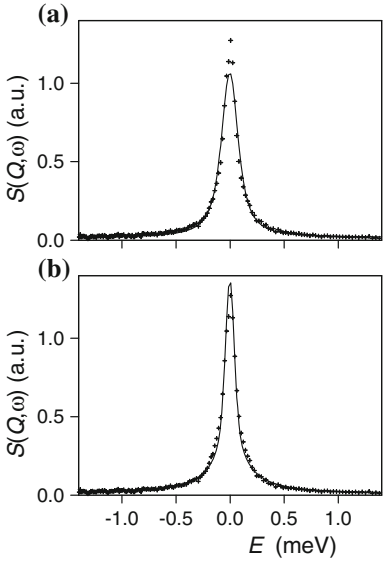

Fig. 2.7 Comparison between experimental (*crosses*) and fitted QENS spectra obtained for H_2 in MIL-47(V) at 77 K. *Solid lines* are computed for **a** three-dimensional diffusion and **b** one-dimensional diffusion (Q = 0.27 Å^{-1}, 3.4 molecules per unit cell on average). The spectra were measured on the IN6 instrument at the ILL. Adapted with permission from (F. Salles, D.I. Kolokolov, H. Jobic, G. Maurin, P.L. Llewellyn, T. Devic, C. Serre, G. Férey, J. Phys. Chem. C **113**, 7802 (2009)) [22]

In MIL-47(V), the reverse is found: The three-dimensional diffusion model reproduces better the QENS spectra than one-dimensional diffusion (Fig. 2.7 and Ref. [22]). The motions of H_2 in this MOF are random because there are no specific adsorption sites for hydrogen.

The D_s values of H_2 in both solids are reported in Fig. 2.8 as a function of loading. Contrary to the concentration dependence obtained in NaX (Fig. 2.4), D_s decreases in both MILs when the H_2 loading increases, this is due to steric reasons in these one-dimensional systems, and to the absence of strong adsorption sites. Experiment and simulation find higher diffusivities in MIL-47(V) than in MIL-53 (Cr), whatever the loading. This can be explained by the presence of the μ_2-OD groups in MIL-53(Cr) which act as attractive sites and steric barriers for H_2, leading thus to a slower diffusion process. Further, a high H_2 mobility is observed in both MILs, at low loading, the D_s values are about two orders of magnitude higher than in zeolites (Fig. 2.4 and Ref. [15]). Extrapolating D_s to zero loading in Fig. 2.8 leads to a value of the order of 10^{-6} m^{2}s^{-1} in MIL-47(V). This is comparable to the supermobility predicted in single-walled carbon nanotubes [24].

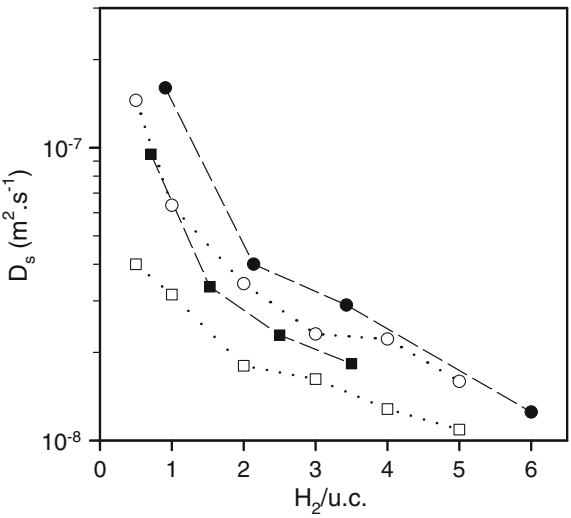

Fig. 2.8 Self-diffusivities of H_2 at 77 K as a function of loading in MIL-47(V) (*rounds*) and MIL-53(Cr) (*squares*): QENS (*full symbols*) and MD (*empty symbols*), where *u.c.* = unit cell

2.3.1.3 Diffusion of Hydrogen in ZIFs

Zeolitic imidazolate frameworks (ZIFs) constitute a sub-family of MOFs. They somewhat bridge the gap between zeolites and MOFs. The structural topologies of ZIFs are similar to zeolite or zeolite-like topologies [25]. ZIFs have tetrahedral frameworks where transition metals (Zn, Co, etc.) are linked by imidazolate ligands, the angle formed by imidazolates when bridging transition metals being close to the Si–O–Si bond angle in zeolites (≈145°). These new materials exhibit exceptional chemical and thermal stability.

Although ZIFs can have large cavities, the windows apertures whereby mass-transport proceeds have rather small diameters. In ZIF-8, the linker between Zn atoms is 2-methylimidazolate, and the diameter of the window is approximately 3.4 Å [25]. The diffusivities computed from MD, even for H_2, have been found to be quite sensitive to the mobility of the linker [26]. This is illustrated in Fig. 2.9, where a comparison between experimental and calculated self-diffusivities shows that an agreement is only reached for a flexible framework. As detailed in Sect. 2.3.2, quantum corrections were included via the Feynman–Hibbs approach [26]. The influence of flexibility on computed diffusivities in ZIF-3, which has a larger window diameter (4.6 Å), was found to be less pronounced, the agreement with QENS values being not as good as in ZIF-8 [26].

2.3.2 Quantum Effects on the Diffusion of Hydrogen Isotopes

Conventional methods for H_2 isotope separation, such as cryogenic distillation or thermal diffusion, are complex and energy intensive. From a classical viewpoint,

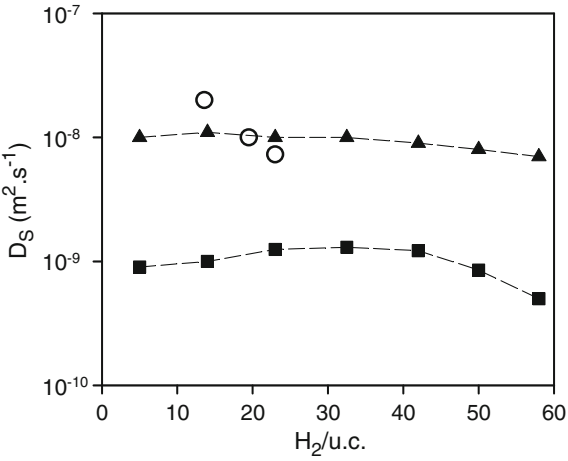

Fig. 2.9 QENS self-diffusivities for H_2 in ZIF-8 at 77 K (*circles*), compared with values computed with a rigid (*squares*) and flexible (*triangles*) framework model

H_2 and D_2 are similar in terms of size and shape as well as energetic considerations. However, H_2 and its isotopes can no longer be treated as classical molecules at low temperatures, as quantum effects become important due to their low mass. Quantum separation should be facilitated by the larger de Broglie wavelength of the lighter isotope. Kinetic molecular sieving, based on differences in diffusivity of the two isotopes, is attractive for porous materials with pore sizes comparable to the de Broglie wavelength.

MD simulations, with quantum corrections incorporated via the Feynman–Hibbs approach, showed that D_2 should diffuse faster than H_2 below 150 K [27], in a hypothetical zeolite rho having a window diameter of 5.43 Å (this corresponding to the distance between the O centres, upon subtraction of the O diameter a free diameter of 2.73 Å is obtained). QENS experiments were performed to test this prediction. However the zeolite rho used for the measurements had a different chemical composition, so that the free diameter of the windows was approximately 3.26 Å [28]. A new set of potential parameters was defined for the MD simulations, which yielded excellent agreement with the QENS diffusion coefficients of H_2 and D_2, but no quantum effect was observed. This was attributed to the larger pore size in the rho sample used experimentally.

Another series of QENS experiments performed with a carbon molecular sieve (CMS) confirmed the predictions made by the simulations [29]. A CMS can be obtained with different pore sizes, and the Takeda 3 Å CMS has pores below 3 Å. In this material, it was indeed found that D_2 diffuses faster than H_2, below 100 K (Fig. 2.10). This shows the extreme sensitivity of the reverse kinetic-selectivity on the window dimension. Transition-state theory and MD calculations indicated that to achieve high flux the cages interconnected by these windows must be small.

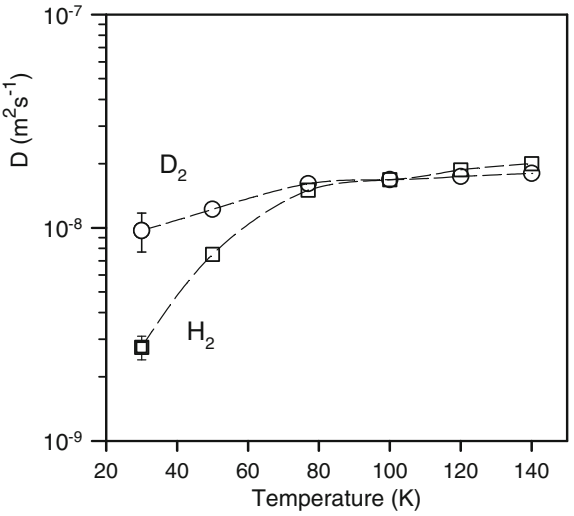

Fig. 2.10 Diffusion coefficients of H_2 (*squares*) and D_2 (*rounds*) in Takeda 3 Å CMS, as a function of temperature (*loading* 0.5 mmol/g)

2.4 Conclusions

Sensitivity is often a problem when studying catalysts with neutrons, only solids which have high surface areas can be studied. One still needs more neutron flux to widen the range of applications.

With INS, the advent of the VISION instrument at the Spallation Neutron Source (SNS) at the Oak Ridge National Laboratory (ORNL), the LAGRANGE instrument being operational at the ILL, and possible improvements on the instrument TOSCA at ISIS should allow us to tackle in the near future grafted catalysts, fuel cells, small supported metal particles (metal loading <1 %), etc. The large Q values which are inherent to these spectrometers at large energy transfers is a serious limitation. The detrimental influence of the Debye–Waller factor on the INS spectra has been known for a long time [30]. This can be partially resolved using direct geometry instruments which allow access of lower Qs [31], but different incident energies have to be selected so that various parts of the spectrum can be combined. On the other hand, the technique is particularly suited to study the different hydrogen species which are formed after dissociation of dihydrogen, during reduction or activation of the catalyst. The problem of characterizing active hydrogen is still a big issue in catalysis.

In the same way as ab initio methods are increasingly being used in INS, molecular simulations are now combined with QENS experiments. Since the space and time scales of the neutron techniques match closely the ones covered by molecular simulations, one expects, and usually finds, good agreement between neutrons and simulations. QENS constitute a benchmark to validate and further develop the modelling work, and the computed trajectories of the sorbate guest molecules within the host matrices are invaluable to understand QENS observables. Discrepancies between experiment and simulation do happen and require in such cases the consideration of a flexible lattice or an improved force field.

References

1. H. Jobic, J. Mol. Catal. A: Chem. **158**, 135 (2000)
2. F. Salles, H. Jobic, G. Maurin, M.M. Koza, P.L. Llewellyn, T. Devic, C. Serre, G. Férey, Phys. Rev. Lett. **100**, 245901 (2008)
3. N. Malikova, S. Longeville, J.-M. Zanotti, E. Dubois, V. Marry, P. Turq, J.M. Ollivier, Phys. Rev. Lett. **101**, 265901 (2008)
4. H. Jobic, in *Catalysis by Metals,* A.J. Renouprez, H. Jobic (eds.) (Les Editions de Physique – Springer, Berlin 1997), p. 181
5. P.W. Albers, S.F. Parker, Adv. Catal. **51**, 99 (2007)
6. A.A. Khassin, G.N. Kustova, H. Jobic, T.M. Yurieva, Y.A. Chesalov, G.A. Filonenko, L.M. Plyasova, V.N. Parmon, Phys. Chem. Chem. Phys. **11**, 6090 (2009)
7. R. Juarez, S.F. Parker, P. Concepcion, A. Corma, H. Garcia, Chem. Sci. **1**, 731 (2010)
8. C. Pirez, M. Capron, H. Jobic, F. Dumeignil, L. Jalowiecki-Duhamel, Angew. Chem. Int. Ed. **50**, 10193 (2011)
9. B. Bogdanovic, M. Schwickardi, J. Alloys Compd. **1**, 253 (1997)
10. C.H. Liu, B.H. Chen, C.L. Hsueh, J.R. Ku, M.S. Jeng, F. Tsau, Int. J. Hydrogen Energy **34**, 2153 (2009)
11. D. Colognesi, A. Giannasi, L. Ulivi, M. Zoppi, A.J. Ramirez-Cuesta, A. Roth, M. Fichtner, J. Phys. Chem. A **115**, 7503 (2011)
12. K. Sköld, G. Nelin, J. Phys. Chem. Solids **28**, 2369 (1967)
13. A. Renouprez, P. Fouilloux, R. Stockmeyer, H.M. Conrad, G. Goeltz, Ber. Bunsenges. Phys. Chem. **81**, 429 (1977)
14. A. Renouprez, R. Stockmeyer, C.J. Wright, J. Chem. Soc. Far. Trans. I **75**, 2473 (1979)
15. N.K. Bär, H. Ernst, H. Jobic, J. Kärger, Magn. Reson. Chem. **37**, S79 (1999)
16. R. Hempelmann, D. Richter, D.A. Faux, D.K. Ross, Z. Phys, Chem. Neue Folge **159**, 175 (1988)
17. L. Onsager, Phys. Rev. **37**, 405 (1931)
18. H. Jobic, D.N. Theodorou, Microporous Mesoporous Mater. **102**, 21 (2007)
19. H. Jobic, J. Kärger, M. Bée, Phys. Rev. Lett. **82**, 4260 (1999)
20. E. Pantatosaki, G.K. Papadopoulos, H. Jobic, D.N. Theodorou, J. Phys. Chem. B **112**, 11708 (2008)
21. P.G. de Gennes, Physica **25**, 825 (1959)
22. F. Salles, D.I. Kolokolov, H. Jobic, G. Maurin, P.L. Llewellyn, T. Devic, C. Serre, G. Férey, J. Phys. Chem. C **113**, 7802 (2009)
23. H. Jobic, K. Hahn, J. Kärger, M. Bée, A. Tuel, M. Noack, I. Girnus, G.J. Kearley, J. Phys. Chem. B **101**, 5834 (1997)
24. A.I. Skoulidas, D.M. Ackerman, J.K. Johnson, D.S. Sholl, Phys. Rev. Lett. **89**, 185901 (2002)
25. R. Banerjee, A. Phan, B. Wang, C. Knobler, H. Furukawa, M. O′Keeffe, O.M. Yaghi, Science **319**, 939 (2008)
26. E. Pantatosaki, H. Jobic, D.I. Kolokolov, S. Karmakar, R. Biniwale, G.K. Papadopoulos, J. Chem. Phys. **138**, 34706 (2013)
27. A.V. Anil Kumar, S.K. Bhatia, Phys. Rev. Lett. **95,** 245901 (2005)
28. A.V. Anil Kumar, H. Jobic, S.K. Bhatia, J. Phys. Chem. B **110,** 16666 (2006)
29. T.X. Nguyen, H. Jobic, S.K. Bhatia, Phys. Rev. Lett. **105**, 085901 (2010)
30. H. Jobic, Chem. Phys. Lett. **106**, 321 (1984)
31. S.F. Parker, D. Lennon, P.W. Albers, Appl. Spectrosc. **65**, 1325 (2011)